ARTICLE

Check for updates

Efficient valley polarization of charged excitons and resident carriers in Molybdenum disulfide monolayers by optical pumping

Sangjun Park [1], Steve Arscott[2], Takashi Taniguchi [3], Kenji Watanabe [4], Fausto Sirotti [1] & Fabian Cadiz [1]✉

The roadmap of future innovative device developments foresees the reduction of material dimensions down to nanometer scale and the incorporation of novel degrees of freedom. For instance, electrons and holes in 2D semiconductors like MoS_2 monolayers exhibit a unique coupling between the spin and the crystal momentum, also referred to as the valley. A crucial requirement for future applications is therefore the possibility to initialise the spin/valley degree of freedom in these materials. Here we investigate the optical initialisation of the valley degree of freedom in charge-tunable MoS_2 monolayers encapsulated with hexagonal boron nitride at cryogenic temperatures. We report in photoluminescence a large steady state valley polarization of the different excitonic complexes following circularly-polarized laser excitation. We reveal efficient valley initialisation of positively-charged excitons, which have so far proved to be elusive in non-encapsulated monolayers due to defect and laser-induced large electron doping. We find that negatively-charged excitons present a polarization of 70% which is unusually large for non-resonant excitation. We attribute this large valley polarization to the particular band structure of MoS_2. In addition, we demonstrate that circular excitation induces a dynamical polarization of resident electrons and holes––as recently shown in tungsten-based monolayers.

[1] Laboratoire de Physique de la Matière Condensée, CNRS, Ecole Polytechnique, Institut Polytechnique de Paris, 91120 Palaiseau, France. [2] University of Lille, CNRS, Centrale Lille, Univ. Polytechnique Hauts-de-France, UMR 8520-IEMN, F-59000 Lille, France. [3] International Center for Materials Nanoarchitectonics, National Institute for Materials Science, 1-1 Namiki, Tsukuba 305-0044, Japan. [4] Research Center for Functional Materials, National Institute for Materials Science, 1-1 Namiki, Tsukuba 305-0044, Japan. ✉email: fabian.cadiz@polytechnique.edu

Two-dimensional crystals of transition metal dichalcogenides (TMD) such as MX_2 (M=Mo, W; X=S, Se, Te) have emerged as promising, atomically-thin semiconductors for applications in valley/spintronics[1–3]. Indeed, the interplay between inversion symmetry breaking in monolayers (ML) and the strong spin-orbit interaction induced by the heavy transition metal atoms yields a unique spin/valley coupling which is expected to provide additional functionalities in future devices[2,4–6]. The absence of inversion symmetry in the single layer limit is also at the origin of chiral optical selection rules which enables an all-optical manipulation and readout of both the valley and spin degree of freedom. Due to enhanced Coulomb interaction in 2D, weak dielectric screening and large effective masses, the optical excitation couples mostly to exciton and trion resonances[7–9]. Remarkably, light absorption due to these strongly bound excitons preserves the coupling between light chirality and the valley. The very first demonstrations of a valley polarization controlled by light helicity in TMDs were obtained using monolayer MoS_2[10–14], the first member of the TMD family to be isolated into a single layer and shown to become a direct bandgap semiconductor- in contrast with the indirect bandgap character of bulk MoS_2[15,16]. The important role played by MoS_2 in early studies is explained by the high abundance of the naturally occurring mineral molybdenite[17]. However in the following years after these key experiments, detailed optical studies on the optical manipulation of the valley degree of freedom focused mainly on monolayer WSe_2 and $MoSe_2$ due to their apparent superior optical quality with respect to MoS_2. Importantly, in these two materials the application of gate voltages allowed one to tune the resident carrier density and therefore to study the valley properties of neutral, positively and negatively charged excitons. In contrast, non-encapsulated MoS_2 suffers from large inhomogeneous broadening and strong photo-induced irreversible changes in the photoluminescence (PL) emission after laser exposure[18,19]. As a result, the PL spectrum of MoS_2 at low temperatures was systematically dominated by negatively charged excitons and electrostatic doping in the hole regime was never achieved. Only very recently electrostatic p-doping was achieved in MoS_2 monolayers encapsulated with hexagonal boron nitride (h-BN)[20]. This encapsulation has been shown to dramatically improve the PL linewidth in TMDs and also prevent unintentional electron doping in MoS_2[21]. The high optical quality provided by h-BN encapsulation had open the door for the observation of dark excitons[22–24], phonon-replicas[25,26], donor-bound excitons[27], neutral and charged bi-excitons[28–30] and, more recently, the well-resolved fine structure of negatively-charged excitons in tungsten-based TMD monolayers[31–33]. This trion fine structure has been recently used to demonstrate efficient valley polarization of resident electrons in WSe_2 and WS_2 monolayers[34].

In this work, we have fabricated a charge-tunable device with encapsulated MoS_2; and we present an investigation of the steady-state valley polarization following circularly-polarized excitation of neutral and charged excitons in all doping regimes. In particular, we find an unusually large valley polarization of negatively-charged trions which we attribute to the unique bandstructure of monolayer MoS_2. In addition, we demonstrate the existence of a dynamical valley polarization of resident electrons and holes, which can be detected as changes in the photoluminescence's intensity of trions when switching from a linearly-polarized to a circularly-polarized laser excitation. This work broadens our understanding on the rich valley physics of excitons and resident carriers in TMD MLs, which is an important step for the development of future valleytronic devices.

Results and discussion

Sample characterization. A charge tunable device such as the one shown in Fig. 1a was fabricated by mechanical exfoliation of bulk MoS_2 crystals from 2D semiconductors. Exfoliation was done inside a glovebox where oxygen and water levels are kept below 1 ppm. 100 nm Au/5nm Ti lines were pre-patterned onto an SiO_2 (90 nm)/Si substrate using lithographic techniques and physical vapor deposition onto which the heterostructure was then deposited by using a transparent viscoelastic stamp[35]. Two graphite flakes were used to contact the MoS_2 monolayer to one of the gold electrodes which permits for an electrostatic doping by the application of a gate bias voltage V_g.

A hyperspectral confocal micro-PL (μPL) set-up is used to excite and detect the polarized exciton emission at cryogenic temperatures[36,37]. The samples are kept inside a closed cycle He cryostat and excited with a continuous wave solid-state laser at 633 nm (~1.96 eV). The polarization of both the laser and the detected PL is controlled with liquid crystal retarders and linear polarizers. The sample temperature is maintained at 20 K. The laser beam is focused onto a diffraction-limited spot (of Gaussian radius $\approx 0.4\,\mu m$) in the sample plane thanks to a vacuum (and cryogenic) compatible, apochromatic objective mounted inside the cryostat (numerical aperture NA = 0.82). The resulting PL spot is imaged onto the entrance slit of a 320 mm focal length spectrometer equipped with a 600 grooves/mm diffraction grating. For micro-reflectivity measurements, an image of a pinhole (diameter 50 μm) illuminated by a quartz-tungsten
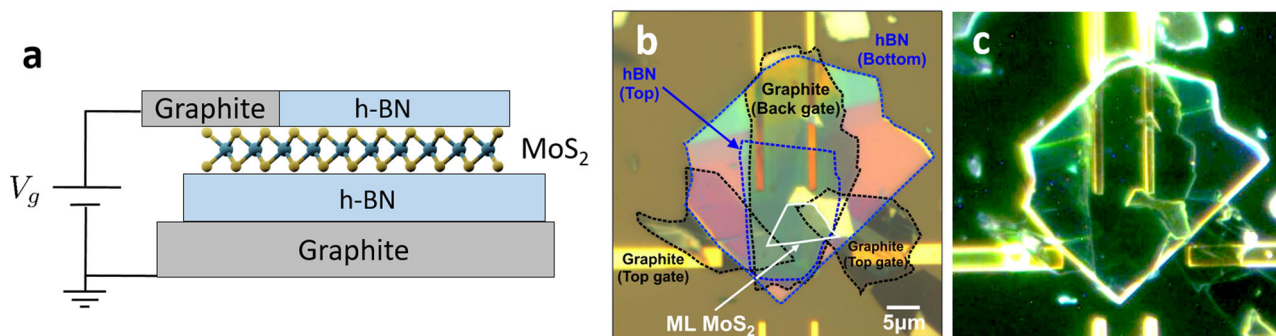

Fig. 1 Charge tunable device based on a MoS₂ monolayer. a Schematic side-view of the sample. The MoS_2 monolayer is encapsulated between two thin h-BN flakes to provide high optical quality and to prevent photodoping effects. Thin graphite flakes were used to provide an electrical control, via the gate bias voltage V_g, of the resident carrier concentration in the monolayer. The whole heterostructure is deposited onto a silicon substrate with a 90 nm-thick silicon dioxide layer on top of which gold lines were deposited lithographically prior to the mechanical exfoliation. **b** Optical microscope image of the sample under white light illumination. **c** Dark-field image of the sample, revealing clean interfaces with no visible bubbles after the formation of the heterostructure. The scale is the same as in panel (**b**).

halogen lamp is formed by the objective into the sample plane, thus probing the reflectivity of the monolayer over a typical diameter of ~1 μm.

Fig. 1 (a) shows a schematic drawing of the charge tunable Van der Waals heterostructure deposited onto a SiO$_2$/Si substrate containing lithographically-defined gold connections. A microscope image of the sample under white light illumination is shown in Fig. 1b, whereas the dark field image of the same region is shown in Fig. 1c. The absence of visible bubbles and wrinkles in the latter image is a signature of the clean interfaces achieved during the transfer process[38,39]. This is confirmed by the well-resolved features observed in the PL spectrum at low temperatures.

As shown previously, encapsulation by h-BN provides linewidths close to the homogeneous limit at low temperatures[21,40,41], allowing for a clear spectral separation of the different excitonic complexes and the study of their valley polarization under circularly-polarized excitation. Moreover, encapsulation allows one to achieve both n and p-doping by the application of a gate voltage, so far inaccessible in non-encapsulated MoS$_2$. Recent scanning tunneling spectroscopy (STS) measurements have shown that h-BN encapsulation moves the Fermi level of monolayer MoS$_2$ closer to the middle of the electronic bandgap, significantly reducing the electron doping when compared to monolayers exfoliated onto SiO$_2$[42]. This is probably due to the fact that h-BN encapsulation inhibits charge transfer between the monolayer and the SiO$_2$, as well as with atoms and molecules that may act as molecular gates when interacting with native defects. Successful p- and n-type doping in our device is demonstrated in Fig. 2a, where the PL spectrum is plotted against the gate voltage under a 10 μW cw excitation. Both positive (X^+) and negatively (X^-) charged trions emerge at positive and negative values of V_g, respectively. Fig. 2b–d shows the PL spectrum at selected voltages together with the differential reflectivity spectrum, defined as $(R_{ML} - R_0)/R_0$, where R_{ML} is the reflected spectrum obtained when illuminating the monolayer with a white light source and R_0 is the reflected spectrum when illuminating all the layers except for the MoS$_2$. The neutral exciton (X^0) PL linewidth in the neutral regime is 4.3 meV. Taking into account the acoustic-phonon broadening of the linewidth[21], this would correspond to ~ 3.2 meV at $T = 4K$ which approaches state-of-the art values and confirms the high optical quality of the sample[43]. In both PL and reflectivity we observe

efficient transfer of oscillator strength from neutral to charged excitons when changing the gate voltage. In the n-type doping regime, the fine structure of the negatively-charged trion manifests itself as the appearance of a double peak[44–46], which we resolve despite the significant broadening of the emission. The solid red line in Fig. 2d is a fit with two Lorentzians, the dashed lines represent each of the two peaks separately. Their energies are found to be 22.4 and 33.3 meV below the X^0 energy in the neutral regime, respectively, whereas the binding energy of the X^+ varies between 24.6 meV (at $V_g = +10V$) and 25.5 meV (at $V_g = +30V$). The bias-dependence of the energies of the different exitonic resonances is the result of bandgap renormalization and screening of Coulomb interactions when charges are added to the system[47,48]. The n-type regime is also accompanied by a 10-fold reduction of the PL yield. This reduction of the PL yield is consistent with recent observations[49], although performed at room temperature. This is not observed in the p-type doping regime, where a moderate broadening is observed but the PL yield is not significantly reduced.

A possible explanation for this asymmetry in the PL yield is the following: in as-exfoliated MoS$_2$ monolayer, it has been observed by scanning tunneling spectroscopy and transport measurements that sulfur vacancies create localized in-gap states that act as hole traps[50,51]. In the n-type doping regime, these localized states can contribute to a fast non-radiative decay channel for the negatively-charged trions. In contrast, in the p-type doping regime these traps are neutralized by capturing holes. This can also explain the emission observed at ~1.8 eV and denoted as X'^+, which probably stems from positive trions in which the recombining hole is bound to one of these traps. Finally, this hole trapping can also explain why in the p-type regime the neutral exciton emission never disapears completely, even at the largest voltages applied. Trapping of holes can indeed limit the maximum density of positive trions that we can achieve in our device. In order to have an estimate of the density of injected electrons and holes, we have performed gate-dependent Raman spectroscopy on the same sample. Figure 2e shows a Raman spectrum in the neutral regime, where the optically active modes E' and A'_1 are clearly visible. Note that the absence of the LA(M) mode in the Raman spectrum (see Supplementary Note 1) allows us to exclude a density of vacancies larger than 10^{12} cm^{-2}[52], which is the typical density of vacancies found in pristine monolayers exfoliated from natural MoS$_2$. Electron (hole) doping
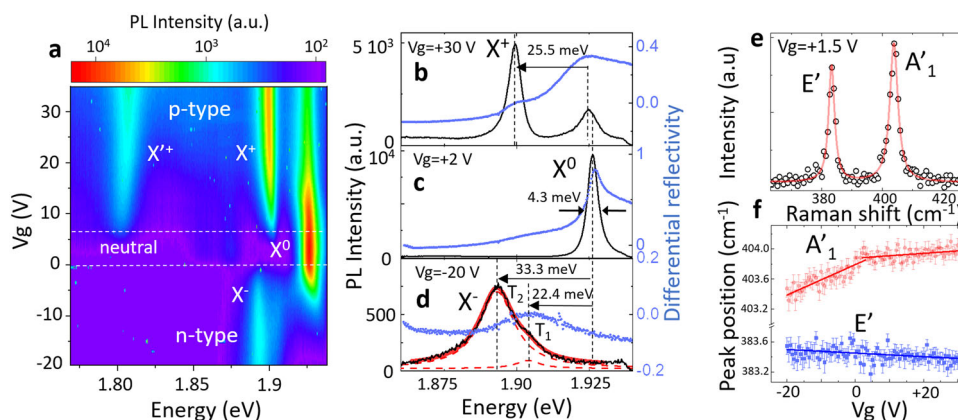

Fig. 2 Optical characterization of a charge tunable MoS$_2$ monolayer. a Photoluminescence (PL) intensity on a logarithmic scale under continuous wave (cw) laser excitation at 10 μW as a function of photon emission energy and gate bias V_g. **b** PL spectrum at a gate voltage corresponding to the p-type regime. **c** PL spectrum at a gate voltage corresponding to the neutral regime. **d** PL spectrum at a gate voltage corresponding to the n-type doping regime. Also shown is the differential reflectivity spectrum (filled dots) for each case. **e** Raman spectrum in the neutral regime, exhibiting the well-known E' and A'$_1$ vibrational modes. **f** Peak position for both modes of panel (**e**) as a function of gate bias. The error bars correspond to the uncertainty given by the fitting of the Raman spectrum with a double Lorentzian.

causes a redshift (blueshift) of the A_1' mode due to change of electron-phonon interactions, whereas E' is almost unaffected[53]. This is confirmed in Fig. 2f which shows the position of both peaks as a function of the gate voltage. In the n-doping regime, the A_1' mode redshifts by $0.5\,\text{cm}^{-1}$ at $V_g = -20$ V, which corresponds to a maximum areal electron density of $n \sim 1.5 \times 10^{12}\,\text{cm}^{-2}$[54], consistent with the absence of the low energy feature observed in[44] which only appears above a density of $4 \times 10^{12}\,\text{cm}^{-2}$. Note that the A_1' peak shifts with a much reduced slope in the p-doped regime, due to a strong electron-hole asymmetry in the softening of the out-of-plane vibrational modes[55]. Assuming that the monotonic increase of the X^+ binding energy with gate bias (see Supplementary Note 3) reflects the position of the Fermi level E_F inside the valence band, we can estimate the hole density achieved at positive $V_g = +30$ V to be $p \sim 3.6 \times 10^{11}\,\text{cm}^{-2}$. Importantly, no significant hysteresis is observed in the behavior of the PL when varying the gate voltage. The neutrality point, defined as the value of V_g for which the X^0 intensity is maximized always occurs at voltages between 2 and 3 V. No change in the PL spectrum is observed after laser exposure, excluding the presence of laser-induced photodoping effects[18].

Valley polarization of neutral and charged excitons. In Fig. 3 we show the polarization-resolved PL intensity in the different regimes (neutral in Fig. 3a, p-type in Fig. 3b and n-type in Fig. 3c) following circularly polarized excitation or linearly polarized excitation at $10\,\mu$W. Also shown is the degree of polarization at each emitted photon energy, defined as $\mathcal{P} = (I_{\text{co}} - I_{\text{cross}})/(I_{\text{co}} + I_{\text{cross}})$ with I_{co} (I_{cross}) the PL intensity co-linearly (crossed) polarized with respect to the laser. Under circular excitation, all the excitonic complexes exhibit high circular polarization, co-linearly polarized with respect to the laser indicating an efficient pumping of the valley degree of freedom in all cases. The degree of circular polarization is similar for X^0, X^+ and X'^+, close to 50% with no strong bias dependence. Surprisingly, the circular polarization of the negatively charged trion complex is significantly higher, around 70%, consistent with some of the very first optical pumping experiments performed in non-encapsulated MoS_2 where a very high steady-state circular polarization of the PL was observed with a He-Ne laser excitation. In early work this high polarization was attributed to the neutral exciton emission, but it has been shown since that photodoping effects lead to heavily electron doped MoS_2 and total quenching of the neutral exciton on silicon substrates. So, those high values of valley polarization agree with what we observe for the negative trion, and the red He-Ne lasers used at the time were in fact

practically unintentionally resonant with the X^0. In the neutral regime, in addition to the neutral exciton peak (X^0), two peaks are clearly visible at lower energies, as shown in Fig. 3a and labelled X'^0 and X''^0. They lie at ~51.3 meV and ~69.5 meV below the neutral exciton, respectively, regardless of the laser excitation energy. Since their intensities follow the same trend as the X^0 when varying V_g (as can be seen in Fig. 1a), and due to their polarization properties and linear dependence on excitation power up to hundreds of μW, we tentatively ascribe them to phonon-assisted recombination of indirect excitons, although more experiments will be required to determine the exact nature of these transitions. These peaks have been observed in several samples and persist up to at least 70 K, more details can be found in the Supplementary Note 2.

When exciting with a linearly polarized laser, a coherent superposition of excitons in the K^+ and K^- valley is generated. Due to the very short exciton lifetime, in the 10^{-12}s range[56–60], this valley coherence is partially preserved before radiative recombination, and so the neutral exciton emission is co-linearly polarized with respect to the laser, with a degree of linear polarization as high as 60%. For all the other peaks, no significant linear polarization is detected. This includes the two additional peaks X'^0 and X''^0 observed in the neutral regime. If they were simply phonon replicas of the X^0, they should exhibit linear polarization as well. We have varied the excitation power by several orders of magnitude between 0.1 and 100 μW. Figure 4a shows that in this power range all the excitonic species are in the linear regime, the continuous line representing a linear relationship between the integrated intensity and the excitation power. In this same power range, the degree of circular polarization is rather stable for all the complexes, but the valley coherence shows a significant drop above several tens of μW, as shown in Fig. 4b.

We will now focus in the very high circular polarization of the negatively charged trion, which is unusual for non-resonance excitation. To explain this, we emphasize that MoS_2 has a unique band structure with respect to other members of the TMD family. Indeed, the small spin-orbit splitting of the conduction band is such that the spin ordering of the conduction subbands in each valley is reversed by interactions in the exciton picture. The upper conduction band having a heavier effective mass, together with the repulsive electron-hole coulomb exchange interaction leads to a "dark" configuration of the lowest energy exciton in monolayer MoS_2, despite the "bright" arrangement of the spin-polarized conduction bands in the single particle picture[61,62]. This dark character of the lowest energy exciton has been confirmed recently in magneto-optic experiments[63]. This, together with the small spin-orbit splitting of the conduction band, makes the
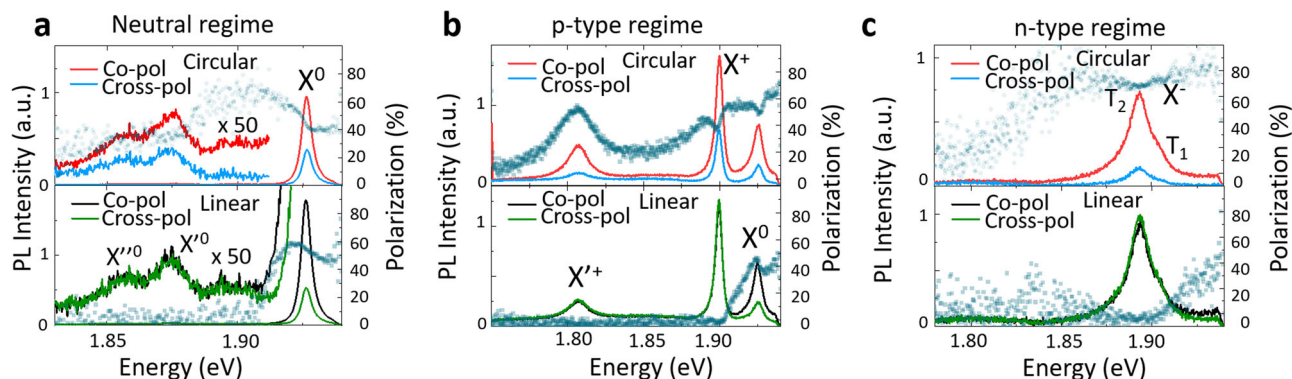

Fig. 3 Polarization behaviour of the photoluminescence. Polarization-resolved photoluminescence (PL) emission under circularly polarized excitation and linearly polarized excitation for different gate voltages, +3V (**a**), +30 V (**b**) and −20 V (**c**). Here the PL components co-polarized and cross-polarized with respect to the laser are denoted by co-pol and cross-pol, respectively. Also shown is the energy-resolved degree of PL polarization (blue dots).
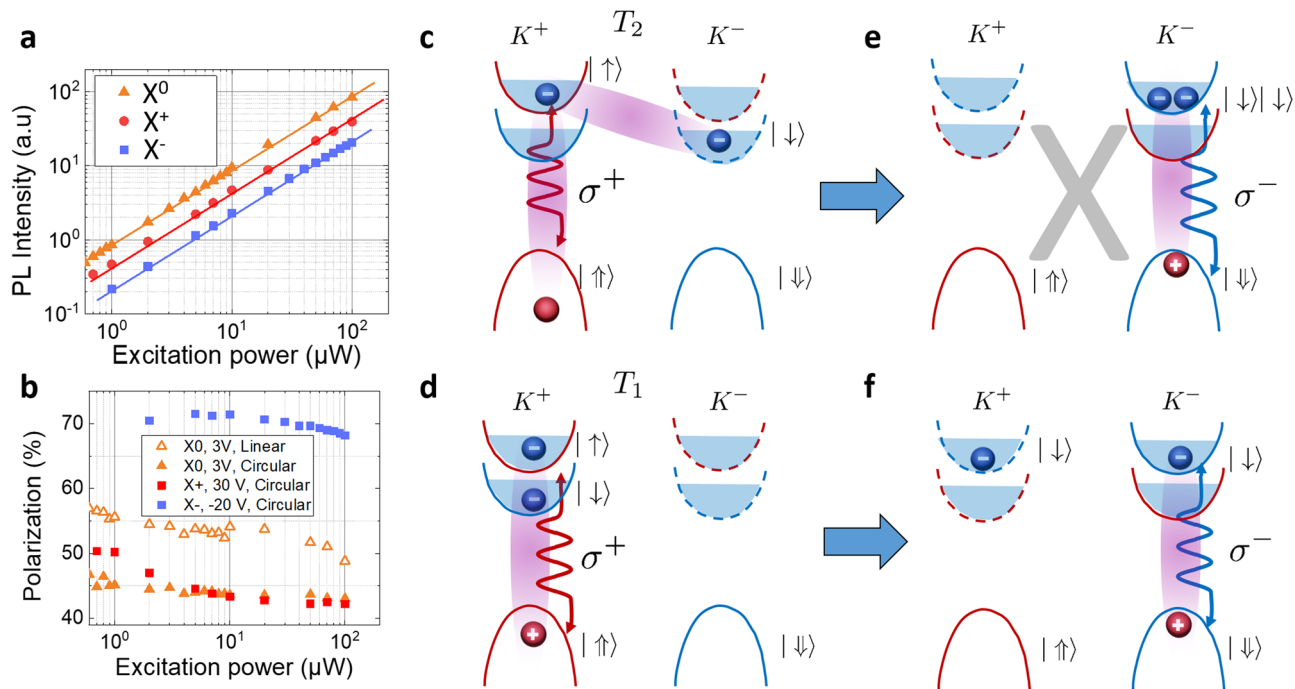
Fig. 4 Bandstructure of MoS$_2$ monolayer and valley relaxation of negatively-charged trions. a Integrated intensity as a function of excitation power. The error bars are two small to be visible and obtained through the fitting procedure of the photoluminescence (PL) intensity of each excitonic peak, which is the limitting factor here due to the high power-stability of the excitation laser. **b** Degree of polarization as a function of excitation power. The error bars are not visible since the error in the polarization is smaller than 1 percent thanks to the laser power stability and callibration of the waveplates. **c** Schematics of a negatively charged trion in the K^+ valley corresponding to a spin singlet state in which both electrons reside at opposite valleys. Here T stands for trion and σ represents a circularly-polarized photon state. **d** Negatively charged trion in the K^+ valley corresponding to a spin singlet state in which both electrons reside in the same valley K^+. **e** State obtained after moving the exciton from the K^+ to the K^- valley for the trion depicted in (**c**). This state is forbidden by the Pauli principle. **f** State obtained after moving the exciton from the K^+ to the K^- valley for the trion depicted in (**d**). The continuous (dashed) lines represent the ordering of the conduction bands in the excitonic (single-particle) picture.

formation of two spin-singlet and one spin-triplet negatively-charged trions possible-at least in principle. In a previous work it has been argued that the triplet configuration is unbound and therefore contributes to the high energy tail of the X^0[64]. This is consistent with the doublet structure observed for the X^- in Fig. 2d, where no third peak is clearly visible. The two peaks observed in our experiments would therefore correspond to the two spin singlets T_1 and T_2, whose configurations in the K^+ valley (coupled to σ^+ light) are represented in Fig. 4c and Fig. 4d, respectively. Here, the continuous (dashed) lines represent the ordering of the conduction bands in the excitonic (single-particle) picture. Since the lowest conduction subband is more likely to be populated at moderate doping densities, the formation of the T_2 is more likely than that of T_1 under light excitation, and so we tentatively ascribe the T_2 to the line that dominates the X^- emission in our experiments. Assuming that what limits the X^- valley lifetime is the exciton scattering between valleys as shown in WSe$_2$[65], we now have the following simple picture that explains the unusually high circular polarization of the X^- in MoS$_2$. For the T_2 in K^+, a change of the exciton valley would correspond to the formation of the complex shown in Fig. 4e, which is forbidden due to the Pauli principle. For the T_1 in K^+, a change in the exciton valley would lead to the formation of a triplet trion shown in Fig. 4f, which is likely to be unbound[64] and, in any case, would recombine at a different energy than that of T_1 and T_2. To obtain emission coming from T_1 and T_2 in the K^- valley after σ^+ excitation would then require, in addition to the exciton intervalley transfer, a simultaneous spin (and momentum) flip of the extra electron. This simultaneous transfer of three carriers can explain the robustness of the valley degree of freedom of the negatively-charged trion in MoS$_2$; making it a very

promising quantum state to store and manipulate information. More detailed experiments with time-resolution and tunable excitation energy could give in the future more insights into the role of excess energy and whether any significant valley relaxation occurs during the trion lifetime.

Optically-induced dynamical valley polarization of resident carriers. We finally discuss the possibility of optically detecting a resident carrier polarization in monolayer MoS$_2$. As shown recently[34], efficient optical valley pumping of resident carriers was demonstrated in n-doped WSe$_2$ and WS$_2$ monolayers with a continuous wave, circularly-polarized excitation. This manifests itself by a laser polarization-dependent PL intensity. Fig. 5a shows the total PL intensity under circular (black) and linear (red) laser excitation in the p-type regime at 10 μW. Also shown is the difference between the two spectra (blue dots). We detect a small but measurable difference, with an excess of intensity for X^0 and X'^+ under circular excitation and a decrease in intensity for the X^+. Note that no difference is detected on the reflected laser intensity, excluding polarization-dependent absorption effects or laser power fluctuations. We have also checked that at low excitation power, no difference is observed in the PL emission between circular and linear excitation, as shown in Fig. 5b. We attribute this behaviour to the manifestation of a dynamical polarization of resident holes induced by the circularly polarized cw excitation. Without light excitation and external magnetic fields, both K^+ and K^- valleys are equally populated by holes. Upon σ^+ photoexcitation, excitons are photogenerated in the K^+ valley, where the electron in the exciton occupies the top conduction band in K^+. This electron can scatter to the K^- valley,

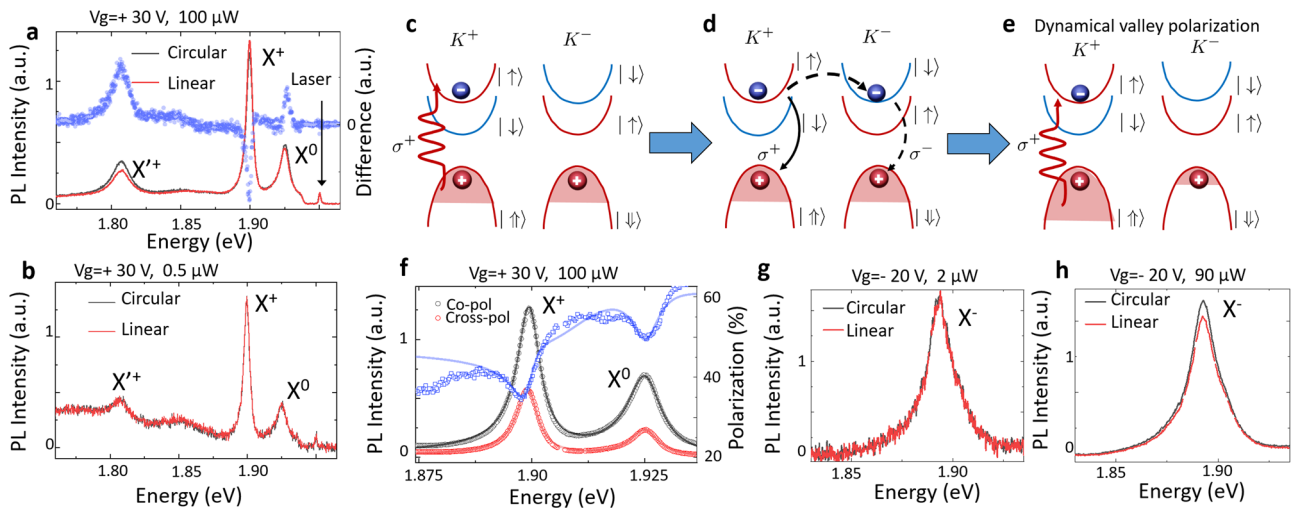**Fig. 5 Optically-induced dynamical polarization of resident carriers in monolayer MoS₂. a** Total photoluminescence (PL) intensity under circular (black) and linear (red) excitation in the p-type regime (gate bias voltage $V_g = +30$ V) at an excitation power of $100\,\mu$W. Also shown in blue dots the difference between these two curves. **b** Same as in (**a**) at a small excitation power of $2\,\mu$W. (**c**) Formation of a positively-charged trion in the K^+ valley following right-handed circular polarization. **d** A trion in the K^+ can either recombine radiatively or scatter to the opposite valley before recombination. **e** In steady state, the process (**c**, **d**) will lead to a spin and valley-polarization of the valence band. **f** Polarized PL emission under circular excitation and degree of circular polarization (blue dots). Co-pol and cross-pol denote the co-polarized and cross-polarized compontents of the PL with respect to the laser, respectively. **g** Total PL intensity under circular (black) and linear (red) excitation in the n-type regime (gate bias voltage $V_g = -20$ V) for an excitation power of $2\,\mu$W. **h** Same as (**g**) for an excitation power of $90\,\mu$W.

eventually recombining with a hole in K^-, resulting in a dynamical buildup of (hole)valley polarization. Another possible mechanism that can contribute to this build-up of valley polarization is illustrated in Fig. 5c–e. Here, an exciton in the K^+ valley binds to a hole in K^- to form the positively-charged trion X^+ (Fig. 5c). This trion can either recombine radiatively in the K^+ valley, in which case no imbalance is created between the valleys, or it can scatter to the opposite valley before recombining. This is represented by the dashed arrows in Fig. 5d. In the latter case, photoexcitation has added a hole to the K^+ valley while substracting a hole in K^-. If the rate of photogeneration is large enough, and if the previously mentioned intervalley scattering mechanisms happens faster than the hole valley relaxation (which can be a very low process due to the significant spin-orbit splitting of the valence bands), this will lead to a larger hole population in K^+ valley, as shown in Fig. 5e. This valley-polarization of the valence bands can qualitatively explain the observations of Fig. 5a: if the X^+ formation is a bimolecular process (exciton binding followed by the capture of an additional hole of the opposite valley), then it is clear that upon circular excitation the X^+ formation is suppressed with respect to the case of linear excitation, resulting in a reduction in the X^+ PL. In contrast, an excess of the X^0 emission is expected since the trion formation rate, a process responsible for exciton dissapearance, will be smaller. The X'^+ intensity being larger under circular excitation is consistent with its assignation to a trion in which the additional hole is trapped by an in-gap state. The formation of this trion is in competition with the formation of the X^+, and so the reduction in X^+ formation rate can favour the formation of X'^+.

In order to estimate the resident hole valley polarization, we use the fact that the X^+ emission energy depends on the position of the quasi Fermi-level of the opposite valley in the degenerate regime. This should produce a splitting of the X^+ emission in σ^+ and σ^- polarization, and therefore an oscillation of the circular polarization inside the X^+ line. This is indeed observed in Fig. 5f, where the polarized PL emission under a circularly-polarized, $100\,\mu$W excitation is shown, together with the degree of circular polarization at each photon energy. The solid lines correspond to

a fit with a double, asymmetrical peak which takes into account the hole recoil effect[66–68]. To fit the σ^+ and σ^- components of the PL, we have kept all the parameters fixed except from the amplitudes and energy positions of each peak. We extract a splitting of the X^+ of $\Delta E = \Delta E_{\sigma^+} - \Delta E_{\sigma^-} = 350 \pm 50\,\mu$eV. The positive sign is consistent with our picture: the emission energy of the σ^+ component should be blueshifted since the quasi-fermi level penetrate less into the K^- valence band. We can roughly estimate the degree of valley polarization by using the previously estimated resident hole density of $p \sim 3.6 \times 10^{11}$ cm^{-2}, which gives, for a temperature $T = 20$ K and a hole effective mass of $m^* \approx 0.5 m_0$, a Fermi level of $E_F^0 \sim 1$ meV below the top of the valence band in the absence of light excitation. Since in each valence band the hole density is given by

$$p^{\pm} = \frac{k_B T m^*}{2\pi\hbar^2} \ln\left(1 + e^{(E_v - E_F^{\pm})/k_B T}\right)$$

with $E_F^{\pm} = E_F^0 + \Delta E/2 = 1 \pm 0.175$ meV, we estimate a hole valley polarization of ~6.3%. This is significantly smaller than the resident carrier valley polarization of 80% achieved in n-doped WSe₂ monolayers, and consistent with the much smaller variations of PL intensity under circular and linear excitation observed here in monolayer MoS₂. The smaller spin-orbit splitting of the valence band in Mo-based TMDs may be at the origin of this smaller steady-state hole valley polarization.

We note that also a small splitting of the X^0 is responsible for a rapid oscillation of the circular polarization inside the exciton line, which is absent in the neutral regime (Fig. 2a). Indeed the valley polarization of the valence band should give rise to a valley-dependent X^0 binding energy. We have found that the asymmetry in the high-energy side of the X^0 line is different for the σ^+ and σ^- components, making a reliable determination of the splitting difficult. Finally, we show in Fig. 5g–e that an optical signature of the valley polarization of resident electrons is also observed in the n-type regime for a sufficiently large excitation power. Here, an easy estimation of the valley polarization is not possible due to the broad emission of the negatively-charged trions. Importantly, these results demonstrate that the dynamical valley polarization

and spin-dependent PL emission is not restricted to tungsten-based TMD monolayers.

Conclusions

In summary, this work broadens our understanding on the different mechanics that may influence the robustness of the valley polarization of quasiparticles in TMD monolayers and the dynamical valley polarization of resident carriers. We have demonstrated p and n-type electrostatic doping in MoS_2 monolayers and study the valley polarization of several excitonic complexes. Several of these complexes have never been reported before. We find large steady-state circular polarization upon circular excitation for all these excitonic complexes. The inverted band ordering between the single particle and the exciton picture is a particular feature of MoS_2 and makes negatively-charged trions in this material very promising candidates for future valleytronic applications, exhibiting high circular polarization in PL emission. We have also demonstrated the signatures of an optically-induced dynamical valley polarization of resident electrons and holes,which can be achieved with continous wave circularly-polarized excitation.This work is thus an important step towards the development of valleytronic devices based on TMD MLs. Indeed, both highly-polarized trions and valley polarized resident carriers influence the transport and the optical properties of TMDs and may be detected and manipulated in experiments such as the valley Hall effect[69].

Methods

Substrate fabrication. Silicon dioxide layers were thermally grown on a 3-inch diameter silicon wafer (100, p-type 5–10 ohm cm) in a tube furnace (dry oxidation conditions). The thickness of the oxide was measured to be 90.1 ± 1.2 nm using ellipsometry (AutoSE spectroscopic ellipsometry, Horiba). Next an ebeam-based lithographic/lift-off microfabrication process was performed involving two thermal evaporation metallization steps to obtain large (500 µm × 500 µm) contact/bonding pads having a Cr/Au thickness of 5/300 nm and long, thin (1 µm or 3 µm) conducting lines having a thickness of 5/50 nm which lead up to the target area for the ML deposition. The thickness of the metallizations was verified using surface profiling (DektakXT - Bruker, USA). The wafers were diced to obtain individual chips measuring 8 mm by 8 mm.

Device fabrication and charge tunable measurements. Prior to the fabrication of the Wan der Waals heterostructure, the substrate was cleaned with acetone and isopropanol (IPA) in an ultrasonic bath for 15 minutes each time to remove the photoresist that was deposited after evaporation of the metal pads for protection. After the transfer of each layer, an annealing was done at 220–230 °C for 30 min in a vacuum chamber to remove residues between the layers. For the annealing, the temperature was increased at a rate of 10°C/min and the pressure was kept below 10^{-7} Torr during the whole process. For the gate-dependent PL measurements, a Keithley 2400 sourcemeter was used with the ground connected to the bottom graphite flake.

Data availability

The datasets generated and/or analysed during the current study are available from the corresponding author on reasonable request.

References

1. Behnia, K. Condensed-matter physics: polarized light boosts valleytronics. *Nat. Nanotechnol.* **7**, 488 (2012).
2. Xiao, D., Liu, G.-B., Feng, W., Xu, X. & Yao, W. Coupled spin and valley physics in monolayers of MoS2 and other group-vi dichalcogenides. *Phys. Rev. Lett.* **108**, 196802 (2012).
3. Butler, S. Z. et al. Progress, challenges, and opportunities in two-dimensional materials beyond graphene. *ACS Nano* **7**, 2898 (2013).
4. Li, L. et al. Room-temperature valleytronic transistor. *Nat. Nanotechnol.* **15**, 743 (2020).
5. Li, L. et al. Electrical switching of valley polarization in monolayer semiconductors. *Phys. Rev. Mater.* **4**, 104005 (2020).
6. Huang, Z. et al. Robust room temperature valley hall effect of interlayer excitons. *Nano Lett.* **20**, 1345 (2020).
7. Ramasubramaniam, A. Large excitonic effects in monolayers of molybdenum and tungsten dichalcogenides. *Phys. Rev. B* **86**, 115409 (2012).
8. Ross, J. S. et al. Electrical control of neutral and charged excitons in a monolayer semiconductor. *Nat. Commun.* **4**, 1474 (2013).
9. Mak, K. F. et al. Tightly bound trions in monolayer mos2. *Nat. Mater.* **12**, 207 (2013).
10. Cao, T. et al. Valley-selective circular dichroism in MoS2. *Nat. Commun.* **3**, 887 (2012).
11. Mak, K. F., He, K., Shan, J. & Heinz, T. F. Control of valley polarization in monolayer MoS2 by optical helicity. *Nat. Nanotechnol.* **7**, 494 (2012).
12. Zeng, H., Dai, J., Yao, W., Xiao, D. & Cui, X. Valley polarization in mos2 monolayers by optical pumping. *Nat. Nanotechnol.* **7**, 490 (2012).
13. Sallen, G. et al. Robust optical emission polarization in MoS2 monolayers through selective valley excitation. *Phys. Rev. B* **86**, 081301 (2012).
14. Kioseoglou, G. et al. Valley polarization and intervalley scattering in monolayer MoS2. *Appl. Phys. Lett.* **101**, 221907 (2012).
15. Splendiani, A. et al. Emerging photoluminescence in monolayer MoS2. *Nano Lett.* **10**, 1271 (2010).
16. Mak, K. F., Lee, C., Hone, J., Shan, J. & Heinz, T. F. Atomically thin MoS2: A new direct-gap semiconductor. *Phys. Rev. Lett.* **105**, 136805 (2010).
17. Dickinson, R. G. & Pauling, L. The crystal structure of molybdenite. *J. Am. Chem. Soc.* **45**, 1466 (1923).
18. Cadiz, F. et al. Ultra-low power threshold for laser induced changes in optical properties of 2D molybdenum dichalcogenides. *2D Mater.* **3**, 045008 (2016).
19. Wierzbowski, J. et al. Direct exciton emission from atomically thin transition metal dichalcogenide heterostructures near the lifetime limit. *Sci. Rep.* **7**, 12383 (2017).
20. Klein, J. et al. Controlling exciton many-body states by the electric-field effect in monolayer MoS2. *Phys. Rev. Res.* **3**, L022009 (2021).
21. Cadiz, F. et al. Excitonic linewidth approaching the homogeneous limit in MoS2 based van der Waals heterostructures : accessing spin-valley dynamics. *Phys. Rev. X* **7**, 021026 (2017).
22. Robert, C. et al. Fine structure and lifetime of dark excitons in transition metal dichalcogenide monolayers. *Phys. Rev. B* **96**, 155423 (2017).
23. Liu, E. et al. Gate tunable dark trions in monolayer WSe2. *Phys. Rev. Lett.* **123**, 027401 (2019).
24. Zinkiewicz, M. et al. Neutral and charged dark excitons in monolayer WS2. *Nanoscale* **12**, 18153 (2020).
25. Liu, E. et al. Valley-selective chiral phonon replicas of dark excitons and trions in monolayer WSe2. *Phys. Rev. Res.* **1**, 032007(R) (2019).
26. Robert, C. et al. Measurement of conduction and valence bands g-factors in a transition metal dichalcogenide monolayer. *Phys. Rev. Lett.* **126**, 067403 (2021).
27. Rivera, P. et al. Intrinsic donor-bound excitons in ultraclean monolayer semiconductors. *Nat. Commun.* **12**, 871 (2021).
28. Chen, S. Y., Goldstein, T., Taniguchi, T., Watanabe, K. & Yan, J. Coulomb-bound four- and five-particle intervalley states in an atomically-thin semiconductor. *Nat. Commun.* **9**, 3717 (2018).
29. Barbone, M. et al. Charge-tuneable biexciton complexes in monolayer wse2. *Nat. Commun.* **9**, 3721 (2018).
30. Ye, Z. et al. Efficient generation of neutral and charged biexcitons in encapsulated WSe2 monolayersziliang. *Nat. Commun.* **9**, 3718 (2018).
31. Courtade, E. et al. Charged excitons in monolayer wse2: Experiment and theory. *Phys. Rev. B* **96**, 085302 (2017).
32. Vaclavkova, D. et al. Singlet and triplet trions in WS2 monolayer encapsulated in hexagonal boron nitride. *Nanotechnology* **29**, 325705 (2018).
33. Lyons, T. P. et al. The valley zeeman effect in inter- and intra-valley trions in monolayer WSe2. *Nat. Commun.* **10**, 2330 (2019).
34. Robert, C. et al. Spin/valley pumping of resident electrons in WSe2 and WS2 monolayers. *Nat. Commun.* **12**, 5455 (2021).
35. Castellanos-Gomez, A. et al. Deterministic transfer of two-dimensional materials by all-dry viscoelastic stamping. *2D Mater.* **1**, 011002 (2014).
36. Favorskiy, I. et al. Circularly polarized luminescence mmicroscopy for the imaging of charge and spin diffusion in semiconductors. *Rev. Sci. Instrum.* **81**, 103902 (2010).
37. Cadiz, F. et al. Exciton diffusion in WSe2 monolayers embedded in a van der waals heterostructure. *Appl. Phys. Lett.* **112**, 152106 (2018).
38. Purdie, D. G. et al. Cleaning interfaces in layered materials heterostructures. *Nat. Commun.* **9**, 5387 (2018).
39. Jain, A. et al. Minimizing residues and strain in 2D materials transferred from pdms. *Nanotechnology* **29**, 265203 (2018).
40. Jakubczyk, T. et al. Radiative limited dephasing and exciton dynamics in MoSe2 monolayers revealed with four-wave mixing microscopy. *Nano Lett.* **16**, 5333 (2016).

41. Martin, E. W. et al. Encapsulation narrows and preserves the excitonic homogeneous linewidth of exfoliated monolayer MoSe2. *Phys. Rev. Appl.* **14**, 021002 (2020).
42. Klein, J. et al. Impact of substrate induced band tail states onthe electronic and optical properties of MoS2. *Appl. Phys. Lett.* **115**, 261603 (2019).
43. Shree, S. et al. High optical quality of MoS2 monolayers grown by chemical vapor deposition. 2D Materials (2020).
44. Kleinet, J. et al. Trions in MoS2 are quantum superpositions of intra- and intervalley spin states. arXiv:2019.06281 (2021).
45. Grzeszczyk, M. et al. Exposing the trion's fine structure by controlling the carrier concentration in hbn-encapsulated MoS2. Arxiv:2012.04459v2 (2021).
46. Jadczak, J. et al. Probing of negatively charged and neutral excitonsin monolayer MoS2. *Nanotechnology* **32**, 145717 (2021).
47. Chernikov, A. et al. Electrical tuning of exciton binding energies in monolayer ws₂. *Phys. Rev. Lett.* **115**, 126802 (2015).
48. Wang, Z., Zhao, L., Mak, K.F. & Shan, J. Probin the spin-polarized electronic band structure in monolayer transition metal dichalcogenides by optical spectroscopy. Nano Letters, Article ASAP (2017).
49. Lien, D.-H. et al. Electrical suppression of all nonradiative recombination pathways in monolayer semiconductors. *Science* **364**, 6439 (2019).
50. Vancso, P. et al. The intrinsic defect structure of exfoliated mos2 single layers revealed by scanning tunneling microscopy. *Sci. Rep.* **6**, 29726 (2016).
51. Ponomarev, E. et al. Hole transport in excoliated monolayer MoS2. *ACS Nano* **12**, 2669 (2018).
52. Mignuzzi, S. et al. Effect of disorder on raman scattering of single-layer MoS2. *Phys. Rev. B* **91**, 195411 (2015).
53. Iqbal, M., Shahzad, K., Akbar, R. & Hussain, G. A review on raman finger prints of doping and strain effect in tmdcs. *Microelectonic Eng.* **219**, 111152 (2020).
54. Chakraborty, B. et al. Symmetry-dependent phonon renormalization in monolayer mos2 transistor. *Phys. Rev. B* **85**, 161403(R) (2012).
55. Sohier, T. et al. Enhanced electron-phonon interaction in multivalley materials. *Phys. Rev. X* **9**, 031019 (2019).
56. Zhu, C. R. et al. Exciton valley dynamics probed by kerr rotation in wse2 monolayers. *Phys. Rev. B* **90**, 161302 (2014).
57. Yan, T., Qiao, X., Tan, P., & Zhang, X. Exciton valley dynamics in monolayer WSe2 probed by ultrafast Kerr rotation. ArXiv e-prints (2015). arXiv:1507.04599 [cond-mat.mes-hall]
58. Wang, G. et al. Valley dynamics probed through charged and neutral exciton emission in monolayer wse₂. *Phys. Rev. B* **90**, 075413 (2014).
59. Glazov, M. M. et al. Spin and valley dynamics of excitons in transition metal dichalcogenide monolayers. *Phys. status solidi (b)* **252**, 2349 (2015).
60. Robert, C. et al. Exciton radiative lifetime in transition metal dichalcogenide monolayers. *Phys. Rev. B* **93**, 205423 (2016).
61. Marinov, K., Avsar, A., Watanabe, K., Taniguchi, T. & Kis, A. Resolving the spin splitting in the conduction band of monolayer MoS2. *Nat. Commun.* **8**, 1938 (2017).
62. Liu, G.-B., Shan, W.-Y., Yao, Y., Yao, W. & Xiao, D. Three-band tight-binding model for monolayers of group-vib transition metal dichalcogenides. *Phys. Rev. B* **88**, 085433 (2013).
63. Robert, C. et al. Measurement of the spin-forbidden dark excitons in MoS2 and MoSe2 monolayers. *Nat. Commun.* **11**, 4037 (2020).
64. Roch, J. G. et al. Spin-polarized electrons in monolayer MoS2. *Nat. Nanotechnol.* **14**, 432 (2019).
65. Singh, A. et al. Long-lived valley polarization of intravalley trions in monolayer WSe2. *Phys. Rev. Lett.* **117**, 257402 (2016).
66. Christopher, J. W., Goldberg, B. B. & Swan, A. K. Long tailed trions in monolayer MoS2: Temperature dependent asymmetry and resulting red-shift of trion photoluminescence spectra. *Sci. Rep.* **7**, 14062 (2017).
67. Zhumagulov, Y., Vagov, A., Gulevich, D. R., Faria Junio, P. E. & Perebeinos, V. Trion induced photoluminescence of a doped MoS2 monolayer. *J. Chem. Phys.* **153**, 044132 (2020).
68. Zipfel, J. et al. Electron recoil effect in electrically tunable MoSe2 monolayers. arXiv.2111.07676 (2021).
69. Mak, K. F., McGill, K. L., Park, J. & McEuen, P. L. The valley hall effect in MoS2 transistors. *Science* **344**, 1489 (2014).

Acknowledgements

Author contributions

S.P. fabricated the charge tunable device and performed the experiments with F.C. The substrate was fabricated by S.A. K.W and T. T. provided the h-BN crystals. F.C. conceived, designed and supervised the experiments. F.C. analyzed the data with S.P. F.C. wrote the manuscript with inputs from S.A. and F.S.

Competing interests

The authors declare no competing interests.

Additional information

Supplementary information The online version contains supplementary material available at https://doi.org/10.1038/s42005-022-00850-1.

Correspondence and requests for materials should be addressed to Fabian Cadiz.

Peer review information *Communications Physics* thanks the anonymous reviewers for their contribution to the peer review of this work. Peer reviewer reports are available.

Reprints and permission information is available at http://www.nature.com/reprints

Publisher's note Springer Nature remains neutral with regard to jurisdictional claims in published maps and institutional affiliations.